Vibrational State-Resolved Study of the $O^- + D_2$ Reaction: Low-Energy Dynamics from 0.25 to 0.37 eV

M. A. Carpenter[†] **and J. M. Farrar***

Department of Chemistry, University of Rochester, Rochester, New York 14627

Received: February 5, 1997; In Final Form: April 23, 1997[⊗]

We present a study of the particle transfer reaction between O^- and D_2 at three collision energies between 0.25 and 0.37 eV. Over this range, the product flux distributions extend over the full range of scattering angles, indicative of collisions in which the atoms remain in close proximity for a significant fraction of a rotational period. The vibrational state populations show the onset of a population inversion, although the partitioning of available energy remains essentially constant at 30%. Vibrationally resolved product angular distributions show that the products formed in the ground vibrational state are distributed with forward and backward peaks, while products excited to $v' = 1$ are forward peaked. At the lowest collision energy of 0.25 eV, a sharp backward peak in $v' = 0$ appears and provides evidence for the critical role that collinear collisions play in traversing the OD^-·D saddle point, where bending motion leads to electron detachment. The low-energy dynamics are controlled by the competition between electron detachment and particle transfer as governed by nuclear motion through the electron continuum. A comparison of the vibrational state distributions with "prior" statistical distributions shows that the experimental data extrapolate to a distribution "colder" than statistical at zero kinetic energy, consistent with the conversion of the bending vibrational energy at the OD^-·D saddle point into electron ejection.

I. Introduction

The reaction of O^- with molecular hydrogen and its isotopomers is one of the simplest anion−neutral systems, and owing to its apparent simplicity as a model for computing reliable potential energy functions for anionic systems, holds great promise as a paradigm for testing dynamical theories on accurate potential energy surfaces. Several reactive channels are accessible to the system, including hydrogen atom and proton transfer, associative and dissociative detachment, and dissociative charge transfer. At low collision energies, the primary reactive processes are hydrogen atom transfer (1) and associative detachment (2):

$$O^- + H_2 \rightarrow OH^- + H + 0.30\ \text{eV} \quad (1)$$

$$\rightarrow H_2O + e^- + 3.60\ \text{eV}^1 \quad (2)$$

The destruction of O^- by H_2 and D_2 has been studied in a number of experiments. In low-energy drift tube measurements where convective flow determines the mobilities of charged particles, radial electron diffusion allows electron detachment to be distinguished from anion production, and the rates for reactions 1 and 2 may be determined independently. Rate measurements by Parkes[2] showed that at thermal energies the associative detachment reaction is the dominant process, a conclusion in agreement with earlier drift tube work.[3] Additional drift tube studies of O^- with H_2 and D_2 from thermal energy to 0.9 eV[4] have demonstrated that the total rate of O^- destruction is independent of energy; the associative detachment channel is dominant at collision energies below 0.3 eV, and the atom transfer reaction is of primary importance at higher collision energies. The overall thermal rate for O^- destruction is approximately $(5-7) \times 10^{-10}$ cm^3 molecule^{-1} s^{-1}, or 40%−50% of the Langevin value.[5]

In the higher energy regime, a few studies employing ion beam techniques have yielded measurements of product energy disposal and angular distributions. Herbst *et al.*[6] employed an ion beam/scattering cell arrangement to examine atom transfer and electron detachment over the collision energy range from 3.6 to 13.2 eV. Cross and collaborators[7] examined the atom transfer channel (1) over a lower collision energy range from 1.2 to 4.7 eV and observed impulsive dynamics that produced forward scattered OD^- products at the higher end of the energy range. The experimental data also suggested that the reaction proceeded through a transient complex living approximately a rotational period at the lower end of this energy range. Earlier work from our own laboratory[8] presented data in contradiction with this conclusion, showing that the reaction proceeds in a direct manner down to 0.5 eV, with the time scale of the reaction only approaching that of a rotational period at energies below 0.37 eV.

Theoretical calculations on the $[H_2O]^-$ surface have been directed largely toward addressing the nature of the binding of the excess electron by the dipole of H_2O[9,10] and have shown that the vertical electron affinity of H_2O is no more than 10^{-4} eV.[11] Early approximate MO calculations[12] were carried out in the vicinity of the electron continuum corresponding to $H_2O + e^-$. A more recent *ab initio* calculation by Werner, Mänz, and Rosmus[13] focused on the stability of the $[H_2O]^-$ anion, but also addressed the nature of the $O^- + H_2$ and $OH^- + H$ channels that led to this species. One of the objectives of the calculation was to elucidate the structure of the $[H_2O]^-$ species detected in mass spectrometry by Nibbering and co-workers.[14] The calculations showed that approaching $O^- + H_2$ reactants correlate to $OH^-(^2\Sigma^+) + H(^2S_{1/2})$ along a collinear $^2\Sigma^+$ surface. This collinear $^2\Sigma^+$ surface has two shallow local minima separated by a barrier. The attraction of the approaching reagents leads to the first shallow well in which O^- is electrostatically bound by the ion−quadrupole interaction to H_2 in a collinear $O^-\cdots HH$ geometry. Hydrogen atom transfer to a second local minimum, identified as collinear $OH^-\cdots H$, occurs

[†] Present address: Baker Chemical Laboratory, Cornell University, Ithaca, NY 14853.

[⊗] Abstract published in *Advance ACS Abstracts,* July 15, 1997.

S1089-5639(97)00457-X CCC: $14.00

over a small barrier. Decomposition of this second complex, which becomes a saddle point in noncollinear geometries, leads to the products $OH^- + H$. The calculations show that bending motion at this saddle point defines the coordinate leading to associative detachment[15,16] forming $H_2O + e^-$. Noncollinear geometries near the $OH^-{\cdot}H$ saddle point access the $H_2O + e^-$ continuum without a barrier. The direct pathway to electron detachment through the $OH^-{\cdot}H$ complex is consistent with the observation that the associative detachment reaction between $OH^- + H$ to form $H_2O + e^-$ occurs at the Langevin rate.[4] The calculations therefore suggest that the $[H_2O]^-$ species observed in mass spectrometry[14] corresponds to an electrostatically bound $O^- \cdot H_2$ or $OH^- \cdot H$ species.

Despite the simplicity of the $O^- + H_2$, system, high-resolution experimental studies allowing detailed comparison with dynamical calculations and assessment of potential energy surface features, particularly in the chemically interesting low-energy regime, have been quite limited in scope. Measurements of the kinetic energy distributions of the electrons emitted in the associative detachment process,[15,17] equivalent to determining the internal energy of the H_2O product, showed that H_2O is formed with high vibrational/rotational excitation. A preliminary report of the dynamics of the atom transfer reaction 1 in the collision energy regime from 0.25 to 1.2 eV has come from our laboratory.[8] In that study, the OD^- product vibrations were resolved by translational spectroscopy, and the results showed that above a collision energy of 0.5 eV the reaction dynamics are direct, yielding forward scattered OD^- products with significant vibrational excitation. As the collision energy decreases, the magnitude of the product vibrational excitation decreases, and the angular distributions for the product ions become more symmetric, although there are some anomalies in specific vibrational states.

The $O^- + D_2$ (H_2) system is isoelectronic with the well-studied $F + D_2$ (H_2) system,[18,19] in which accurate potential energy surfaces have been calculated[20] and extensive dynamical calculations, both classical[21] and quantum,[22] have been performed. Those studies have served as benchmarks for neutral−neutral reaction dynamics, providing some of the most stringent tests of *ab initio* theory and dynamical theories of reaction dynamics. With the same number of electrons as the $F + H_2$ system, the $O^- + D_2$ system is similar in complexity to its neutral counterpart. The present study is intended to provide similar opportunities to test structural and dynamical approaches to simple particle transfer reactions in anionic systems.

In this paper we present a full account of vibrational energy disposal and product angular distributions for the reactively scattered OD^- products of reaction 1 over the range from 0.25 to 0.37 eV. The data include vibrational state distributions at each collision energy and angular distributions for individual quantum states of the products. The present paper is part of a series of reports on the dynamics of this important reaction: in subsequent papers we will report on the transition to direct dynamics at collision energies from 0.47 to 1.20 eV, as well as on the role of rotational energy consumption in the reagents and disposal in the products.

II. Experimental Section

The crossed beam apparatus used for this study has been described in detail in previous publications.[23] We produced O^- ions by electron impact on N_2O at a pressure of ~0.01 Torr. Following acceleration and momentum analysis by a 60° magnetic sector, the beam was refocused and decelerated to ground potential. The ion beam laboratory energy distribution was approximately triangular in shape, with a full-width at half-maximum of ~0.25 eV. Center of mass collision energies ranging from 0.25 to 0.37 eV required lab energy beams ranging from 0.92 to 1.50 eV. The neutral beam was produced by expanding 560 Torr of D_2 at 300 K through a 0.07 mm nozzle, collimating the beam to 2° by a 1 mm electroformed skimmer and a 3.5 mm square aperture, and modulating it at 30 Hz. Under these conditions, we estimate that the D_2 rotational temperature is 195 K,[24] and the rotational energy of the D_2 reagents is only 0.01 eV.

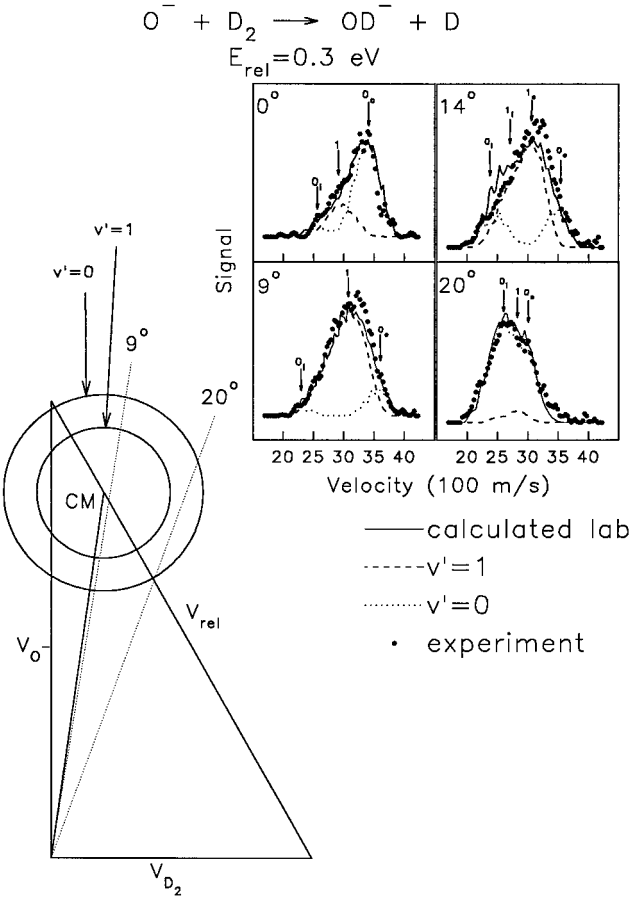

Figure 1. Experimental data for OD^- lab flux distributions at selected laboratory angles at a collision energy of 0.30 eV. At each lab angle, structure in the fluxes is assigned to specific vibrations. The integer above the arrow pointing to a given structure identifies the vibrational quantum number of the OD^- product appearing at that angle and velocity. The subscripts "i" and "o" denote the inner and outer branches of the kinematic circles shown on the Newton diagram. The results of the kinematic simulation of the data are shown at each angle, with contributions from individual vibrational states indicated.

The beams intersected at the center of a collision chamber maintained at 10^{-7} Torr with oil diffusion pumps. Reaction products were detected with a rotatable electrostatic energy analyzer (resolution 0.07 eV)−quadrupole mass filter equipped with a dual microchannel plate ion detector. Data were collected with a multichannel scaler synchronized with the beam modulation as described in our earlier publications.[25] The energy scale was calibrated at the beginning and at the end of each experiment by resonant charge transfer from NO^-, also produced by electron impact on N_2O, to NO expanded supersonically in the crossed beam. This calibration procedure generated a low-energy marker at the energy of the neutral beam, ~0.09 eV. All experimental data were duplicated, and experiments in which the energy of the primary ion beam drifted by more than 0.1 eV were discarded.

III. Results and Analysis

The particle transfer reaction 1 was studied at collision energies of 0.25, 0.30, and 0.37 eV. At each collision energy,

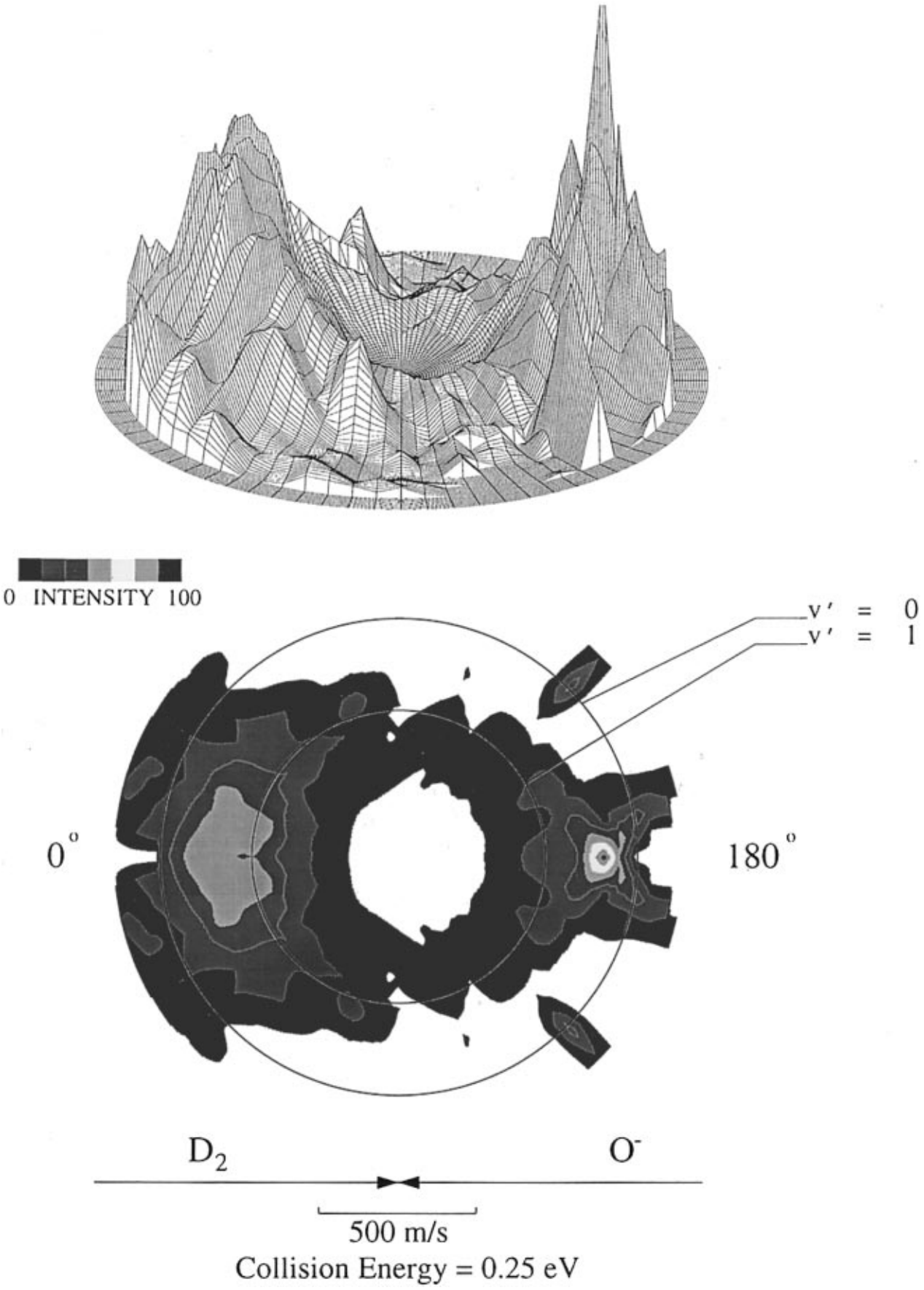

Figure 2. Axonometric plot and color projection of center of mass flux in center of mass velocity space at a collision energy of 0.25 eV. Circles of constant radius corresponding to the loci of points followed by OD^- products formed in the given vibrational state with no rotational excitation are superimposed on the color projection.

laboratory kinetic energy spectra were obtained at a set of 12−15 fixed lab scattering angles. Each energy spectrum consisted of 80 or 120 points, with typical energy bin widths of 0.025−0.03 eV, compared to the laboratory resolution of 0.07 eV. This procedure resulted in a data set consisting of 960−1800 data points covering laboratory velocity space. Figure 1 shows

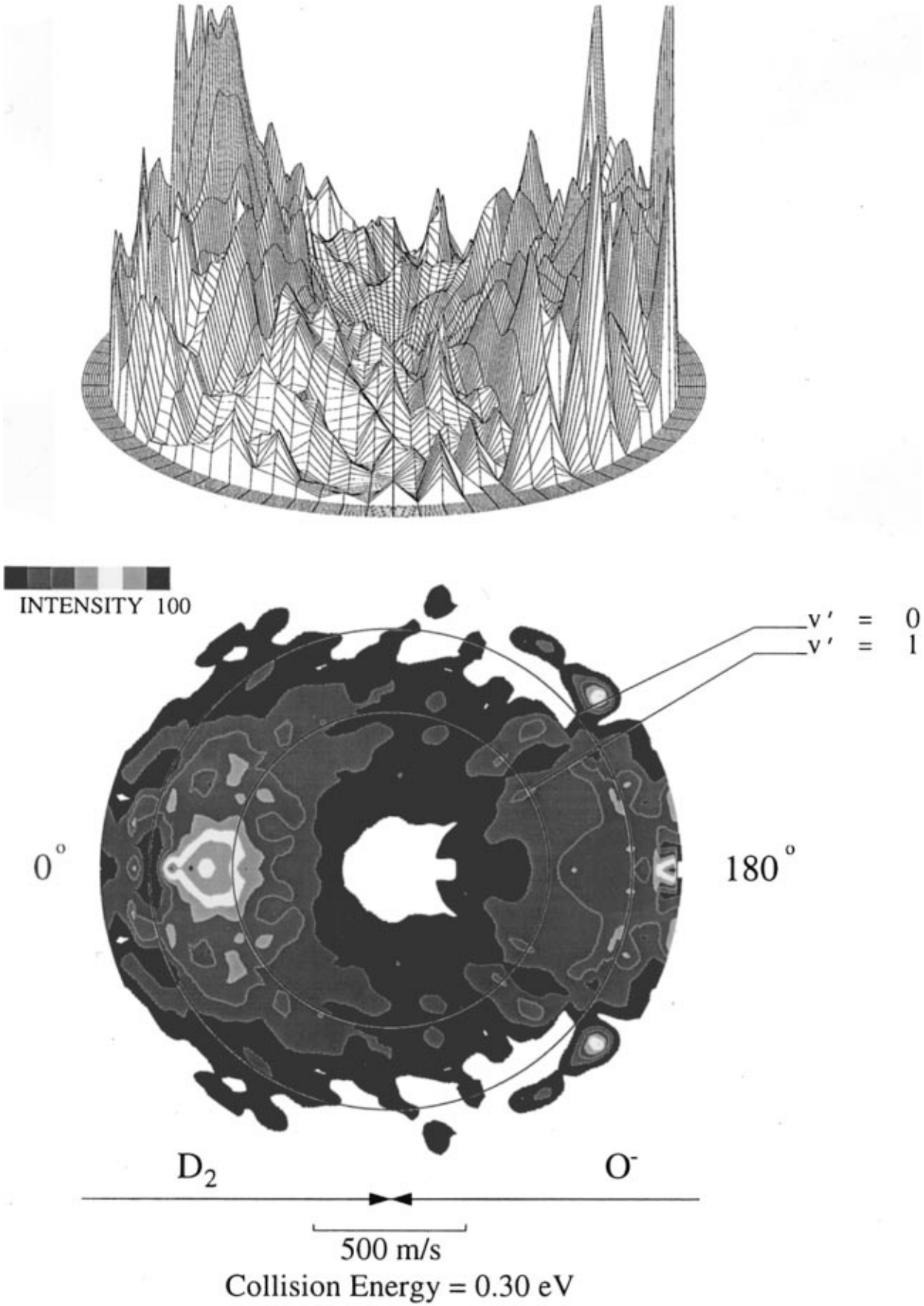

Figure 3. Same as Figure 2, at a collision energy of 0.30 eV.

typical experimental data for the OD^- product fluxes at selected laboratory scattering angles at a collision energy of 0.30 eV. The data are compared with the results of a kinematic simulation of the center of mass distributions that have been transformed back to the laboratory system with appropriate averaging over the experimental conditions. The details of this kinematic calculation will be discussed in later paragraphs. As evident from the Newton diagrams, the ray representing a given

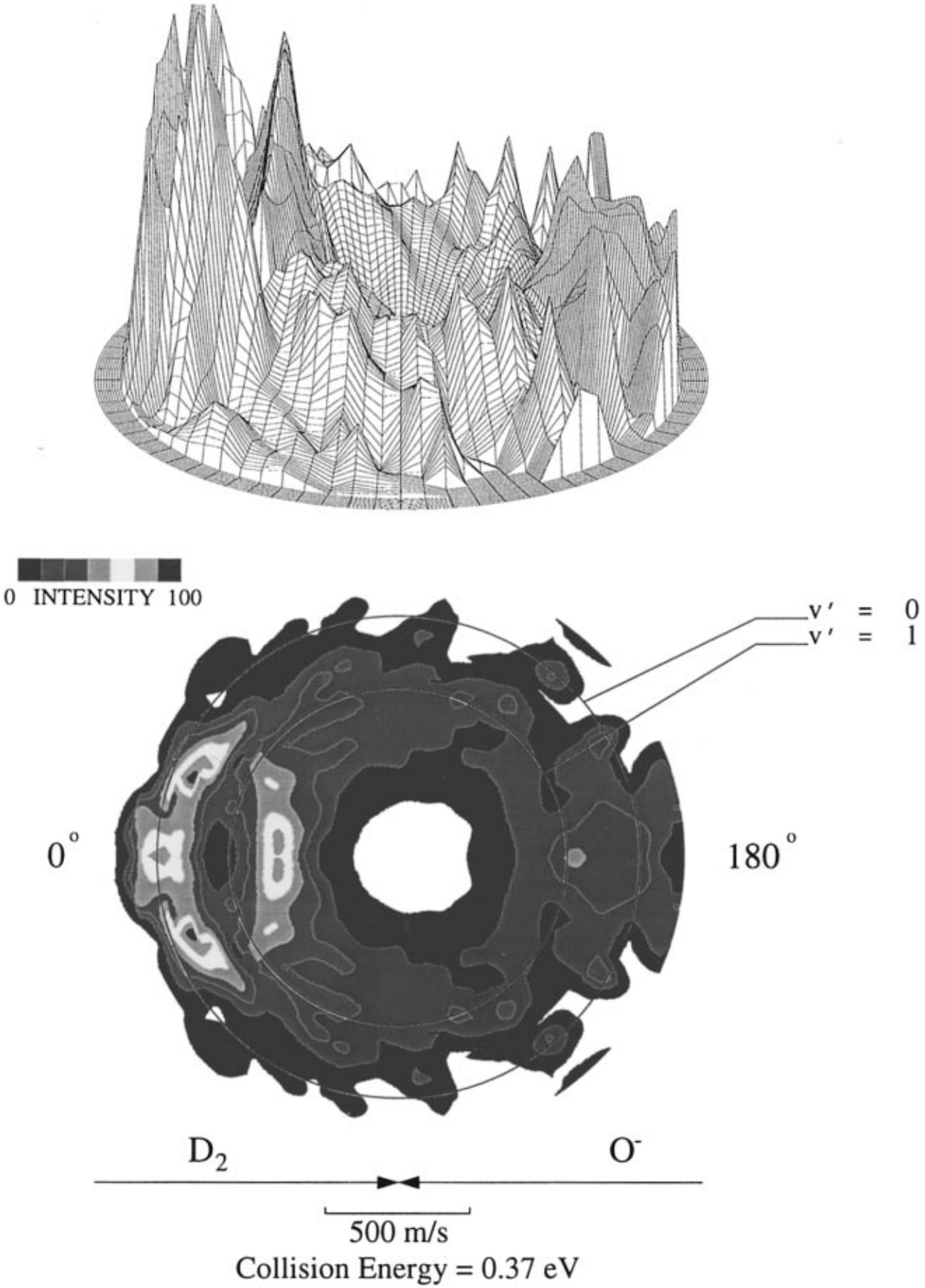

Figure 4. Same as Figure 2, at a collision energy of 0.37 eV.

laboratory angle intersects the manifold of concentric circles corresponding to the center of mass velocities of OD^- products containing discrete quanta of vibrational excitation. The structure in the experimental data corresponds to OD^- produced with specific amounts of vibrational energy and allows us to extract angle-dependent cross sections for individual product vibrational states.

A. Kinematic Analysis. The objective of the data analysis program is to find the unique center of mass cross section $I_{c.m.}(u,\theta)$ that when transformed to the laboratory system with

suitable averaging over the beam velocity distributions, the distribution of beam intersection angles, and the energy resolution of the detector, recovers the experimental data within their intrinsic error limits. As a starting point for extracting dynamical information from the experimental data, we transformed the laboratory flux distributions to the center of mass coordinate system with a pointwise iterative deconvolution procedure.[26] The energy-independent differential cross section $I_{c.m.}(u,\theta)$ is recovered from the lab data by inverting the transformation relation 3 with concomitant removal of the dispersion in beam

$$I_{lab}(V,\Theta) = \sum_{i=1}^{N} f_i \frac{V^2}{u_i^2} I_{c.m.}(u_i,\theta_i) \qquad (3)$$

velocities. The summation extends over a grid of N Newton diagrams that represents the dispersion in beam velocities and intersection angles; the i^{th} diagram is weighted by the value f_i. A grid of 125 Newton diagrams, five in each velocity distributions and five in the distribution of beam intersection angles, provides a thorough average over the dispersion in initial conditions. This procedure allows us to extract a center of mass cross section that when transformed to the laboratory coordinate system with appropriate averaging over the beam widths, recovers the experimental data with a standard deviation of 6−8%. This procedure employs a linear bivariate interpolation algorithm to calculate values of the deconvoluted flux on a grid of center of mass intensities $I_{c.m.}(u,\theta)$ defined by the set of points in lab velocity space at which the experimental data were acquired. We then employ a linear interpolation routine to construct a set of data points on a polar grid in center of mass velocity space. The center of mass intensity distribution $I_{c.m.}(u,\theta)$ generated this way is intrinsically nonseparable in the variables u and θ.

In Figures 2, 3, and 4, we plot the center of mass distributions for the OD^- products. The data are plotted as a function of the polar coordinates u and θ; the vertical coordinate corresponds to the flux intensity at a particular set of polar coordinates. The data plotted in these figures are the direct results of pointwise deconvolution of the experimental data and embody the noise of the original data amplified by the deconvolution procedure. The "tight" kinematics of the $O^- + D_2$ mass combination, *i.e.*, the disparity between the masses of the reactants, result in the formation of products over a restricted region of laboratory coordinates. The finite beam velocity and angular dispersions and detector resolution result in some "spill" of the center of mass fluxes outside of boundaries defined by energy conservation. For example, in Figure 4, the backward scattered peak for the $v' = 0$ product state of OD^- falls outside the kinematic circle for that state. In laboratory coordinates, those products have very low kinetic energy, and the combination of their low energies and the kinematic compression of the data is responsible for the shift of the peak away from the circle corresponding to products formed in the $v' = 0$, $J' = 0$ state.

This representation of the data allows immediate assessment of the reactive dynamics. As the collision energy decreases, the extent of product vibrational excitation decreases. At collision energies of 0.37 and 0.30 eV, the cross sections appear reasonably symmetric with respect to the bisector of the relative velocity vector, and the scattering is distributed over all center of mass angles, although biased toward the forward direction. At the lowest collision energy, the distribution is quite broad and extends throughout the entire range of scattering angles. However, now we observe a very sharp spike in the backward direction corresponding to the formation of OD^- in $v' = 0$. We will show that this latter feature is particularly diagnostic of the low-energy dynamics.

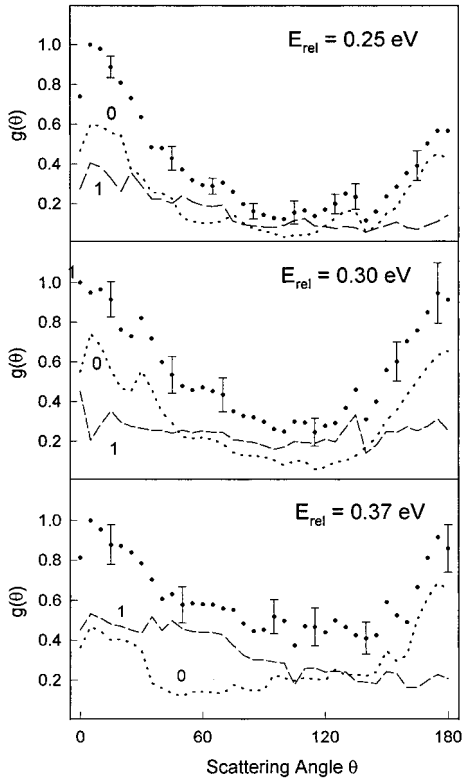

Figure 5. Angular distributions for each vibrational state, 0.25, 0.30, 0.37 eV experiments, obtained from kinematic analysis. Vibrational states are labeled: $v' = 0$ (- - -); $v' = 1$ (− − −). The total angular distribution is indicated by filled circles with error bars.

In order to extract product vibrational states along with their angular dependences from the center of mass distributions, we also reconstructed the laboratory flux distributions by fitting the deconvoluted center of mass fluxes to a series of Gaussian functions indexed to the individual product vibrational states.[27] This procedure treated the center of mass flux distributions as separable product functions in recoil speed and scattering angle in small wedges of center of mass angular space,[28] typically 5−10° in width. By allowing these product functions to vary with scattering angle, the coupling of recoil speed with scattering angle in the data could be recovered accurately. Because the contribution of a given vibrational state in the center of mass system was represented by an analytic function, the contribution of that vibration to the flux in laboratory space could be accounted for directly. The kinematic calculations that are compared with experimental data in Figure 1 are calculated with this fitting procedure. In addition, by integrating the function assigned to a particular vibration at a fixed center of mass scattering angle over the full range of center of mass speeds accessible to products in that vibrational state, the product state-resolved angular distributions $g^{v'}(\theta)$ can be constructed. The product state-resolved angular distributions extracted from the center of mass data for $v' = 0$ and 1 are plotted in Figure 5.

The form of the kinetic energy distribution within a single vibrational state provides information on the distribution of rotational energy within that vibration. The kinematic analysis procedure allows us to extract the range of J' values populated in a given vibrational state. The discussion of rotational energy partitioning in the products and disposal of reagent rotation will be presented in a separate publication.

B. Product State Distributions and Energy Partitioning. The probability of populating a given vibrational state is calculated by integrating the differential cross section, determined either from deconvolution of the laboratory data or by fitting the deconvoluted data to a set of Gaussian functions

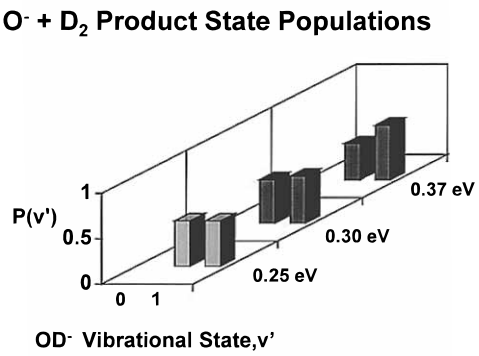

Figure 6. OD^- vibrational state distributions at each collision energy, calculated from eq 4. Error bars are indicated.

representing the contributions from individual vibrational states, over the full range of center of mass scattering angles, and over the range of center of mass speeds accessible to that vibrational state:

$$P(v') = \int_{u_{min}}^{u_{max}} \int_0^{2\pi} I_{cm}^{v'}(u,\theta) \sin\theta \, d\theta \, du \qquad (4)$$

The results of this calculation are shown in Figure 6. At 0.25 eV, the two accessible product vibrational states are populated essentially equally, but increases in collision energy to 0.30 and 0.37 eV result in a slow but distinct shift of population from $v' = 0$ to $v' = 1$. Both the functional fitting approach to extracting the vibrational state-resolved center of mass fluxes and integration of the center of mass function extracted from deconvolution resulted in product state populations in good agreement with one another.

The vibrational state populations allow us to evaluate the fraction of the total available energy appearing in product vibrational energy. We define this fraction by the variable f_V' as follows:

$$f_V' = \frac{\sum_{v'=0}^{v'_{max}} P(v') \, E(v')}{E_{total}} \qquad (5)$$

In this equation, $P(v')$ represents the probability of observing a vibrational state of energy $E(v')$, and E_{total} is the total energy accessible to the system, the sum of reagent translational and internal energy and the reaction exothermicity. For these experiments, f_V' remains constant at approximately 30%.

IV. Discussion

The experimental data reported for this reaction are quite extensive, providing several incisive probes of the nature of collisions leading to reaction over this range of energies. The discussion will focus first on the product vibrational state distributions and their evolution with collision energy. The data also allow us to extract angular distributions for the formation of each product vibrational state at each collision energy, information that provides additional important insight into details about collision lifetimes over the full range of energies. The relationship of the experimental data to specific features of the potential surface will form the basis for much of the discussion. An especially important topic for discussion will be the competition between particle transfer and electron detachment, which provides insight into the role of bending motion in the vicinity of the OD^-·D saddle point.

A. Vibrational State Distributions. Within the narrow collision energy range of these experiments, the OD^- vibrational state distributions evolve subtly but significantly, beginning a trend that is strongly accentuated at higher collision energies.[29] At collision energies of 0.25 and 0.30 eV, the data show that the two lowest vibrational states are populated equally within the uncertainty in the data. A simple phase space calculation,[31] in contrast, shows that the ratio of $v' = 0$ to $v' = 1$ should favor the $v' = 0$ state by a factor of 2:1 and that ratio varies only slowly with collision energy. At 0.37 eV, the experimental data show that the $v' = 0$ to $v' = 1$ ratio is now 40:60, indicating the initial stages of population inversion. At the same time, the phase space calculation still favors the production of the lowest energy $v' = 0$ state by nearly a factor of 2.

Information theory in the form of surprisal analysis[30] provides a simple moment expansion of the product state distributions that allows us to correlate the characteristics of the populations with only a few physically significant parameters. The vibrational surprisal, $I(v')$, is defined in terms of the measured probability of observing a given vibrational state, $P(v')$, in comparison with the "prior" statistical expectation for the population of that state, given as $P_0(v')$:

$$I(v') = -\ln[P(v')/P_0(v')] \qquad (6)$$

The surprisal describes the extent of the deviation of the measured distribution from the least biased or least surprising distribution, the microcanonical distribution in which all microstates at a fixed energy are equally probable. The flux distributions suggest that OD^- products arise from collisions in which all three atoms interact strongly for a significant fraction of a rotational period, akin to a transient complex, and therefore comparisons with statistical "prior" distributions are sensible. We have constructed the vibrational surprisal for the OD^- product states from the measured product state distributions and from prior distributions computed by phase space theory.[31] We find that the surprisal plot slopes, λ_V, are negative at all three collision energies, indicative of a population inversion. The magnitude of the slope is proportional to the "temperature" of the distribution, and we find that the surprisal slopes decrease in magnitude from -1.76 to -1.26 to -0.84 as the collision energy drops from 0.37 to 0.30 to 0.25 eV. The vibrational distributions clearly "cool" monotonically with decreasing collision energy, but do not reach the statistical limit of zero surprisal at 0.25 eV. Significantly, the surprisal slope extrapolates to a positive value at zero collision energy, indicative of a dynamical constraint operative in this collision energy range that places less energy in vibration than expected statistically. We will see that electron detachment becomes a dominant channel in this same low-energy regime and that the branching between detachment and particle transfer is determined by the vibrational motion of the system as it passes through local minima and transition states. This additional dynamical constraint at low energy will be critical in understanding the low-energy product state and angular distributions.

As an initial point for discussing the vibrational energy partitioning of this system, it is useful to consider the reaction dynamics that one expects for the heavy + light−light (H + LL) mass combination appropriate to $O^- + D_2$.[32−34] The attractive long-range force in the entrance channel for this system, providing an example of the "early downhill" potential energy surface, immediately suggests that much of the energy of the reaction is liberated while the reagents approach. This situation leads to the formation of forward scattered, vibrationally excited products through large impact parameter collisions. In addition, numerous trajectory studies on neutral−neutral systems with this mass combination show that a significant fraction of reactive trajectories liberate the energy of reaction while both the breaking bond in the reagent and the newly forming bond of the incipient products are extended. Such

a situation is termed mixed energy release and also leads to the formation of vibrationally excited products. Corner-cutting trajectories characteristic of mixed energy release arise because the skew angle of the potential energy surface for this mass combination is moderate, approximately 48°.[35] At low collision energies, this acute skew angle dictates that most trajectories do not need to be guided into the exit channel by the "corner" of the surface where both the breaking bond and forming bond are compressed. Instead, product trajectories enter the exit valley transverse to the reaction coordinate and form vibrationally excited products.

The behavior of the $O^- + D_2$ system is very similar to that of the $O^- + HF$ system at low collision energies.[36] In the latter system, incremental translation at the lowest collision energies leads to enhanced product vibrational excitation, and the explanation for that behavior has been attributed to the influence of the strong attractive well in preventing trajectories from entering the "corner", but rather transferring the proton at distances in which both the forming bond and breaking bond are extended. The wider skew angle of the $O^- + D_2$ surface relative to that for $O^- + HF$ (48° vs 20°) may be responsible for corner-cutting and the transformation of incremental reagent translation into product vibration in the present system as well.

B. Angular Distributions. In addition to the energy dependence of the product vibrational state distribution, the product angular distributions are one of the key dynamical signatures that unify these three experiments. The angular distributions shown in Figure 5 are qualitatively similar in that they show significant components of scattering both into the forward and backward hemispheres. This behavior provides qualitative indications that the collisions leading to particle transfer in this energy regime are characterized by strong interaction among all three particles on a time scale comparable to the rotational period of the transient $[D_2O]^-$ complex.

We note that the $v' = 0$ level consistently shows forward−backward symmetry over this energy range, while the $v' = 1$ level has a much flatter distribution that rises slightly in the forward direction. Although the $v' = 0$ angular distributions show both forward and backward peaks of comparable heights, the forward peak is broader and the integrated intensity in the forward range of scattering angles, $0 \leq \theta \leq \pi/2$, is 65% of the total. The asymmetry of an angular distribution provides an important insight into the decay rate of the transient intermediate created by the approaching collision partners. When a microcanonical ensemble of transient complexes decays to form products, the decay is characterized by a distribution of lifetimes that becomes random in the statistical limit.[37] The random lifetime distribution favors the shortest lifetimes, and those lifetimes belong to species that decay by the most exothermic channels.[38] In the case of OD^- formed from decay of a $[D_2O]^-$ complex, that part of the ensemble forming $v' = 0$ should decay most rapidly. If that time scale is shorter than a rotational period of the decaying transient, then the angular distribution for that product will be asymmetric.[39] From the statistical viewpoint then, OD^- formed in $v' = 1$ should originate from that part of the ensemble having longer lifetimes, enhancing the probability that those products will have more symmetric angular distributions. In fact, the reactive dynamics behave in exactly the opposite manner. Although the surprisal analysis suggests that the reaction behaves more statistically in the sense that the vibrational surprisal plot slopes approach, but do not reach, zero with decreasing collision energy, the finer details of the dynamics suggest a more subtle transition at low energy.

The form of the product angular distribution at the lowest collision energy of 0.25 eV provides a particularly strong piece of evidence for dynamical specificity as contrasted with statistical behavior. The polar flux plot of Figure 2 shows that although the products are scattered over a wide range of angles and velocities, suggesting superficially that the dynamics are controlled by the decay of a transient complex, the most prominent feature of the flux distribution is a *backward* scattered spike for the formation of OD^- in $v' = 0$. Although integration of the flux shows that forward scattered flux is favored over backward scattered products by a factor of 2, the sharp spike in the backward direction shows that a specific collision geometry in which the reagents must approach in a collinear manner with essentially zero impact parameter and proceed through a "tight", structured transition state is quite important at this collision energy. We would therefore expect the extreme low collision energy limit of the product angular distribution, at least classically, to be backward scattering. As we will discuss later, this low-energy behavior reflects the competition between particle transfer and electron detachment. Both the transit time through the region of the potential surface where these processes compete and the nature of internal excitation in the reaction complex determine the nature of the branching. This competition effectively prohibits reactive trajectories from exploring regions of phase space in which the intermediate complex has bending excitation with periods comparable to or longer than the transit time through the region of the surface where the electron continuum is accessible. The small fraction of collisions that take place through collinear trajectories therefore excludes large volumes of phase space at low collision energies. Such a condition is manifestly nonstatistical and plays a dominant role in the low-energy partitioning and product angular distributions.

D. Potential Energy Surface. A number of the qualitative characteristics of the dynamics of the $O^- + D_2/H_2$ particle transfer reaction can be correlated with known features of the potential surface. Although the surface of Werner *et al.* is not quantitatively correct, its qualitative features are of value in correlating the observed dynamics. The saddle point in the vicinity of the $OH^-\cdot H$ intermediate is particularly important in determining the branching of products between electron detachment and particle transfer. In addition, the energy dependence of the product angular distributions is determined by motion through this region of the surface. A reactive trajectory at low collision energy following the minimum energy path along the potential surface passes through a "tight" complex in which O^- is electrostatically bound to H_2 in a collinear geometry by the charge−quadrupole interaction. This complex is located at a true local minimum on the potential surface. Following hydrogen atom transfer over a small barrier, the minimum energy pathway then leads to the collinear $OH^-\cdot H$ complex. Unlike the $O^-\cdot H_2$ complex, the $OH^-\cdot H$ species is located at a saddle point on the potential surface. Bending motion here lowers the energy of the system, allowing the system to access the associative electron detachment continuum. Figure 7 illustrates schematically the nature of the reaction coordinate in the vicinity of two minima.

Trajectories that follow the minimum energy pathway and maintain collinear geometry throughout the collision result in particle transfer, and the signature of such collisions is the formation of backward scattered OH^-. The observation of a sharp peak in the backward direction in the lowest energy experiment at 0.25 eV is precisely what we would expect from such collinear collisions. The fact that particle transfer products are distributed over a wide angular range in addition to the backward spike indicates that a distribution of impact parameters contributes to reactive collisions. The issue of how nonzero impact parameter collisions proceeding through bent complexes

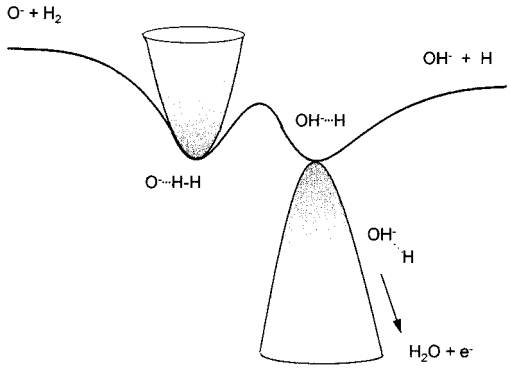

Figure 7. Schematic reaction coordinate, for $O^- + H_2$, showing that the first minimum corresponding to $O^-\cdots H-H$ is a true local minimum, while the second minimum, corresponding to $OH^-\cdots H$ is a saddle point. Bending excitation accesses the electron continuum, forming $H_2O + e^-$ by associative detachment.

and transition states lead to particle transfer rather than electron detachment requires us to consider the theory of associative electron detachment, described in the next paragraph.

Collisions that pass through the region of the $OH^-\cdot H$ complex along trajectories other than the collinear minimum energy pathway may access the electron detachment continuum, but the probability of detachment also depends on the transit time of the system through this critical region of the surface. The local complex potential model,[40] developed to describe electron detachment in diatomic systems, discusses nuclear motion of a bound system embedded in a continuum of electron translational energy levels as governed by the real part $U(R)$ of a potential energy function written as follows:

$$V(R) = U(R) - \frac{i}{2}\Gamma(R) \tag{7}$$

The imaginary term $\Gamma(R)$, a measure of the strength of the coupling of the discrete electronic state to the electron continuum, determines the decay rate. The lifetime with respect to detachment is defined in terms of the autoionization width as $\hbar/\Gamma(R)$. Within this picture, the probability that detachment occurs in the interval of nuclear coordinates (R_i, R_f) is given by

$$P(R_i,R_f) = 1 - \exp\int_{R_i}^{R_f} \frac{2\Gamma(R)}{\hbar V_r}\,dR \tag{8}$$

where V_r is the radial velocity of the nuclei.[41] This expression shows that as the nuclear velocities increase and the transit time through the detachment region becomes short with respect to the autoionization lifetime, the detachment probability decreases. As generalized to polyatomic systems and applied to the competition between detachment and particle transfer in the $O^- + H_2$ system, this expression suggests that at low collision energy, where the nuclear velocities result in transit times comparable to $\hbar/\Gamma(R)$, only the small fraction of collisions that follow the minimum energy path and maintain a collinear geometry result in particle transfer. From the perspective of classical mechanics, in the zero collision energy limit all particle transfer products will be backward scattered in center of mass coordinates. Any trajectory traversing the electron continuum in a bent configuration will undergo detachment. At low collision energy, the preponderance of nonzero impact parameter collisions will cause detachment to be the dominant reactive process. As the collision energy increases, noncollinear trajectories traverse the autoionization region in a time short compared to the detachment lifetime. Trajectories that are also able to "turn the corner" on the potential surface will thus lead to particle transfer. Qualitatively, we expect that larger impact parameter collisions should result in an increased tendency for forward scattering. This interplay of impact parameter, collision geometry, and transit time through the electron detachment continuum leads to the expectation that particle transfer products should be backward scattered in the low-energy limit, with increasing components of forward scattering as the collision energy increases, precisely as we observe.

Although many ion−molecule reactions that appear to proceed as direct processes at hyperthermal collision energies exhibit a transition toward statistical behavior in the low collision energy limit, many features of the $O^- + D_2$ reaction argue against such a simplistic interpretation. The most salient of these arguments is the fact that at the lowest collision energies where electron detachment occurs, large volumes of phase space corresponding to noncollinear trajectories of O^- with respect to the D−D bond axis are inaccessible to the particle transfer products. The embedding of nuclear bound states within the electron translational continuum presents a serious theoretical challenge that must be met in order to understand the key structural and dynamical components determining the outcome of this reaction.

V. Conclusions

We have presented extensive experimental data on the particle transfer reaction taking place between O^- and D_2 over three collision energies between 0.25 and 0.37 eV. Over that range, the vibrational state populations show the onset of a population inversion; the surprisal slopes are negative, with a value of −0.84 at 0.25 eV, increasing monotonically in magnitude to −1.76 at the highest collision energy. The partitioning of available energy into product vibration remains constant at 30%. At a fixed collision energy, the formation of vibrationally excited products is consistent with the mixed energy release motif in which particle transfer takes place under conditions in which both the breaking and forming bonds are extended. However, the partitioning of incremental reagent translation into product vibration is inconsistent with the mass combination, suggesting that subtleties of the potential surface topology control this facet of energy partitioning. Vibrationally resolved product angular distributions show that the products formed in the ground vibrational state are distributed with forward and backward peaks, while products excited to $v' = 1$ are forward peaked. At the lowest collision energy of 0.25 eV, a sharp backward peak in $v' = 0$ appears and provides evidence for the critical role that collinear collisions play in traversing the region of the surface where electron detachment occurs, in the vicinity of the $OD^-\cdot D$ saddle point. A consideration of known features of the potential surface suggests that noncollinear trajectories may branch to electron detachment or particle transfer, depending on the comparison of transit time with Fourier components of the imaginary part of the potential.

The data reported here are among the most detailed available for an ion−molecule collision system. Their interpretation will require a detailed description of the potential energy surface for reaction ranging from the low-energy repulsion to local minima and saddle points describing intermediates separating reactants from products, as well as the critical role of regions of the surface where bound nuclear motions are embedded in the continuum for electron detachment. In addition to the surface, dynamical calculations on the surface will be required for a complete understanding of this system. We hope the present data will stimulate such calculations.

Acknowledgment. We gratefully acknowledge the many contributions of Professor Yuan T. Lee to our understanding of chemical reaction dynamics and dedicate this paper to him.

We acknowledge support of this work by the U.S. Department of Energy. M.A.C. expresses thanks to the University of Rochester for Fellowship support from the Sherman Clarke and Weissberger Funds. We thank Marty Zanni, Susan Troutman Lee, and David Sperry for their assistance in the performing and analysis of these experiments. J.M.F. wishes to thank Professor Richard N. Zare for helpful comments and Professors Franco Vecchiocattivi, Enzo Aquilanti, Piero Casavecchia, and Antonio Laganà of the University of Perugia for continuing conversations. He also acknowledges a NATO Collaborative Research Grant.

References and Notes

(1) Heats of formation are tabulated in: Lias, S. G.; *et al. J. Phys. Chem. Ref. Data* **1988**, *17* Suppl. 1.

(2) Parkes, D. A. *J. Chem. Soc., Faraday Trans. 1* **1972**, 613.

(3) Moruzzi, J. L.; Phelps, A. V. *J. Chem. Phys.* **1966**, *45*, 4617. Moruzzi, J. L.; Eakin, J. W.; Phelps, A. V. *Ibid.* **1968**, *48*, 3070.

(4) Fehsenfeld, F. C.; Howard, C. J.; Ferguson, E. E. *J. Chem. Phys.* **1973**, *58*, 5841.

(5) For a discussion of classical ion−molecule capture theory, see: Su, T.; Bowers, M. T. In *Gas Phase Ion Chemistry*; Bowers, M. T., Ed.; Academic: New York, 1979; Vol. 1, p 84.

(6) Herbst, E.; Payne, L. G.; Champion, R. L.; Doverspike, L. D. *Chem. Phys.* **1979**, *42*, 413.

(7) Johnson, S. G.; Kremer, L. N.; Metral, C. J.; Cross, R. J., Jr. *J. Chem. Phys.* **1978**, *68* 1444.

(8) Carpenter, M. A.; Zanni, M. T.; Farrar, J. M. *J. Phys. Chem.* **1995**, *99*, 1380.

(9) Garrett, W. R. *Phys. Rev. A* **1971**, *3*, 961; *J. Chem. Phys*. **1980**, *73*, 5721; *Ibid*. **1982**, *77*, 3666.

(10) Crawford, O. H. *Mol. Phys.* **1971**, *20*, 585; *Ibid.* **1973**, *26*, 139.

(11) Chipman, D. M. *J. Phys. Chem.* **1978**, *82*, 1080.

(12) Claydon, C. R.; Segal, G. A.; Taylor, H. S. *J. Chem. Phys.* **1971**, *54*, 3799.

(13) Werner, H.-J.; Mänz, U.; Rosmus, P. *J. Chem. Phys.* **1987**, *87*, 2913.

(14) DeKoning, L. J.; Nibbering, N. M. M. *J. Am. Chem. Soc.* **1984**, *106*, 7971.

(15) Mauer, J. L.; Schulz, G. J. *Phys. Rev. A* **1972**, *7*, 593.

(16) Allan, M. *Chimia* **1982**, *36*, 457.

(17) Esaulov, V. A.; Champion, R. L.; Grouard, J. P.; Hall, R. I.; Montmagnon, J. L.; Penent, F. *J. Chem. Phys.* **1990**, *92*, 2305.

(18) Neumark, D. M.; Wodtke, A. M.; Robinson, G. N.; Hayden, C. C.; Lee, Y. T. *J. Chem. Phys.* **1985**, *82*, 3045. Neumark, D. M.; Wodtke, A. M.; Robinson, G. N.; Hayden, C. C.; Shobatake, K.; Sparks, R. K.; Schafer, T. P.; Lee, Y. T. *J. Chem. Phys.* **1985**, *82*, 3067.

(19) Faubel, M.; Rusin, L. Y.; Schelmmer, S.; Sondermann, F.; Tappe, U.; Toennies, J. P. *J. Chem. Phys.* **1995**, *101*, 2106. Faubel, M.; Martinez-Haya, B.; Rusin, L. Y.; Tappe, U.; Toennies, J. P. *Z. Phys. Chem.* **1995**, *188*, 197. Faubel, M.; Martinez-Haya, B.; Rusin, L. Y.; Tappe, U.; Toennies, J. P. *Chem. Phys. Lett.* **1995**, *232*, 197.

(20) Knowles, P. J.; Stark, K.; Werner, H.-J. *Chem. Phys. Lett.* **1991**, *185*, 555. Stark, K.; Werner, H.-J. *J. Chem. Phys.* **1996**, *104*, 6515.

(21) Aoiz, F. J.; Bañares, L.; Herrero, V. J.; Sáez Rábanos, V. *Chem. Phys. Lett.* **1994**, *218*, 422. Aoiz, F. J.; Bañares, L.; Herrero, V. J.; Sáez Rábanos, V.; Stark, K.; Werner, H.-J. *Ibid*. **1994**, *223*, 215.

(22) See, for recent examples: Launay, J. M.; LeDourneuf, M. *Chem. Phys. Lett.* **1990**, *169*, 473. Castillo, J. F.; Manolopoulos, D. E.; Stark, K.; Werner, H.-J. *J. Chem. Phys.* **1996**, *104*, 6531. Neuhauser, D.; Judson, R. S.; Jaffe, R. L.; Baer, M.; Kouri, D. J. *Chem. Phys. Lett.* **1991**, *176*, 546. Zhang, J. Z. H. *Ibid.* **1991**, *181*, 63. Mielke, S. L.; Lynch, G. C.; Truhlar, D. G.; Schwenke, D. W. *Ibid.* **1993**, *213*, 10.

(23) Varley, D. F.; Levandier, D. J.; Farrar, J. M. *J. Chem. Phys.* **1992**, *96*, 8806.

(24) Gallagher, R. J.; Fenn, J. B. *J. Chem. Phys.* **1974**, *60*, 3487, 3492.

(25) Varley, D. F.; Levandier, D. J.; Farrar, J. M. *J. Chem. Phys.* **1992**, *96*, 8806.

(26) Siska, P. E. *J. Chem. Phys.* **1973**, *59*, 6052.

(27) The details of the procedure are given in: Carpenter, M. A. Ph.D. dissertation, University of Rochester, 1996. Published by University Microfilms.

(28) Carpenter, M. A.; Zanni, M. T.; Levandier, D. J.; Varley, D. F.; Farrar, J. M. *Can. J. Chem.* **1994**, *72*, 828.

(29) Carpenter, M. A.; Farrar, J. M. *J. Phys. Chem*.; to be submitted.

(30) Levine, R. D.; Bernstein, R. B. *Acc. Chem. Res.* **1974**, *12*, 393. Levine, R. D.; Bernstein, R. B. *J. Chem. Phys.* **1972**, *57*, 434. Levine, R. D.; Kinsey, J. L. In *Atom-Molecule Collision Theory: A Guide for the Experimentalist;* Bernstein, R. B., Ed.; Plenum: New York, 1979; p 693.

(31) Pechukas, P.; Light, J. C.; Rankin, C. *J. Chem. Phys.* **1966**, *44*, 794. Chesnavich, W. J.; Bowers, M. T. *Ibid.* **1977**, *66*, 2306.

(32) Polanyi, J. C.; Schreiber, J. L. *Faraday Discuss. Chem. Soc.* **1977**, *62*, 267.

(33) Kuntz, P. J.; Nemeth, E. M.; Polanyi, J. C.; Rosner, S. D.; Young, C. E. *J. Chem. Phys.* **1966**, *44*, 1168.

(34) Polanyi, J. C. *Acc. Chem. Res.* **1972**, *5*, 161.

(35) Eyring, H.; Polanyi, J. C. *Z. Phys. Chem*. **1931**, *B12*, 279. Mahan, B. H. *J. Chem. Educ.* **1974**, *51*, 308, 377.

(36) Knutsen, K.; Bierbaum, V. M.; Leone, S. R. *J. Chem. Phys.***1992**, *96*, 298.

(37) Bunker, D. L. *Theory of Elementary Gas Reaction Rates;* Pergamon: Oxford, U.K.; 1966; p 51. Thiele, E. *J. Chem. Phys.* **1962**, *36*, 1466; *Ibid.* **1963**, *38*, 1959.

(38) Holbrook, K. A.; Pilling, M. J.; Robertson, S. H. *Unimolecular Reactions*, 2nd ed.; Wiley-Interscience: Chichester, U.K.; 1996.

(39) Miller, W. B.; Safron, S. A.; Herschbach, D. R. *Faraday Discuss. Chem. Soc.* **1967**, *44*, 108. Fisk, G. A.; McDonald, J. D.; Herschbach, D. R. *Ibid.* **1967**, *44*, 228; Stolte, S.; Proctor, A. E.; Bernstein, R. B. *J. Chem. Phys.* **1976**, *65*, 4990. Bullitt, M. K.; Fisher, C. H.; Kinsey, J. L. *Ibid.* **1974**, *60*, 478.

(40) Herzenberg, A. *Phys. Rev.* **1967**, *160*, 80.

(41) Massey, H. S. W. *Negative Ions*, 3rd ed.; Cambridge University Press: Cambridge, U.K., 1976; p 516.